JACS
JOURNAL OF THE AMERICAN CHEMICAL SOCIETY

Article

pubs.acs.org/JACS

Strained Cyclophane Macrocycles: Impact of Progressive Ring Size Reduction on Synthesis and Structure

Andrew R. Bogdan,[†] Steven V. Jerome,[‡] K. N. Houk,*[,‡] and Keith James*[,†]

[†]The Scripps Research Institute, 10550 North Torrey Pines Road, La Jolla, California 92037, United States

[‡]Department of Chemistry and Biochemistry, University of California, Los Angeles, California 90095-1569, United States

Supporting Information

ABSTRACT: The synthesis, X-ray crystal structures, and calculated strain energies are reported for a homologous series of 11- to 14-membered drug-like cyclophane macrocycles, representing an unusual region of chemical space that can be difficult to access synthetically. The ratio of macrocycle to dimer, generated *via* a copper catalyzed azide−alkyne cycloaddition macrocyclization in flow at elevated temperature, could be rationalized in terms of the strain energy in the macrocyclic product. The progressive increase in strain resulting from reduction in macrocycle ring size, or the introduction of additional conformational constraints, results in marked deviations from typical geometries. These strained cyclophane macrocyclic systems provide access to spatial orientations of functionality that would not be readily available in unstrained or acyclic analogs. The most strained system prepared represents the first report of an 11-membered cyclophane containing a 1,4-disubstituted 1,2,3-triazole ring and establishes a limit to the ring strain that can be generated using this macrocycle synthesis methodology.

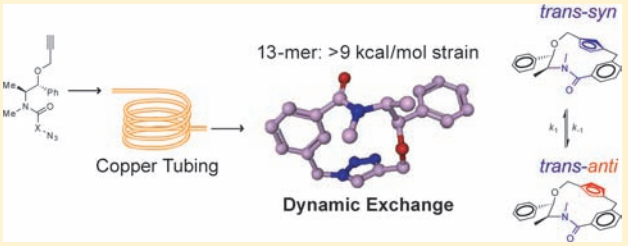

INTRODUCTION

There is growing interest in the design of macrocyclic drugs as a strategy to address challenging biological targets, such as protein−protein interfaces.[1] Although often biologically compelling, these targets are rarely amenable to small-molecule modulation.[2] Macrocycles offer both pharmacological and physicochemical advantages over acyclic molecules with regard to modulation of these problematic molecular targets. The pharmacological advantage stems from the preorganization of bioactive conformations, thereby avoiding entropic losses upon binding that would decrease affinity. Numerous examples of the successful application of this concept have been reported.[3] The physicochemical advantages of macrocycles result from their shape,[1] lower rotatable bond count,[4] and, in some cases, their ability to conceal polar functionality by forming stable, intramolecular hydrogen bonds in low dielectric environments.[5] However, despite these potential advantages, the design of macrocycle-based drugs represents an emerging field, since the synthetic challenges of constructing macrocycles have impeded progress in the area.[6] All current macrocyclic drugs are either natural product-based or cyclic peptides.[7]

An impressive recent chemo-informatic analysis of biologically active macrocycles defines them as organic molecules containing a nonbridged cycle of 12 or more covalently connected atoms.[8] This analysis also revealed that macrocycles represented 2.8% of a database of 130 000 natural products and that, of these, rings containing 14 atoms were most common and fewer than 1% had ring sizes larger than 40 atoms. The construction of macrocyclic rings *via* cyclization of a linear precursor is problematic in that the chemistry of the cyclization is also the chemistry of oligomerization. Consequently, macrocyclizations are typically run at high (ca. 1 mM) or very high (<ca. 1 mM) dilution in order to slow the rate of intermolecular reactions.[7] However, this is inefficient in terms of solvent consumption and reaction time, particularly on a large scale. The problem is amplified in the case of macrocycles at the lower end of the defined ring size, where the strain in the macrocyclic product results in a slower macrocyclization rate and therefore a low yield of macrocycle compared to the product of the undesired, but less strained, intermolecular reaction. In some cases, this can render the macrocyclization unobservable.[9] The strain energy of these 'small ring' macrocycles results from distortion of standard bond angles and lengths associated with enclosure in a ring. In addition, rings of this size can experience unfavorable transannular interactions between substituents on opposite sides of the ring.

Consequently, small strained macrocycles represent an intriguing region of chemical space that can be difficult to access chemically. They have the potential to yield unusual molecular shapes, unconventional bond geometries, and spatial orientations of functional groups that are quite different from unstrained or acyclic systems. When such macrocycles also possess the functionality and physicochemical properties typical of drug molecules, they offer access to drug-like molecular diversity that is quite distinct from that usually found in corporate or public domain screening files. These strained

Received: September 8, 2011
Published: December 1, 2011

   dx.doi.org/10.1021/ja208503y | *J. Am. Chem.Soc.* 2012, 134, 2127−2138

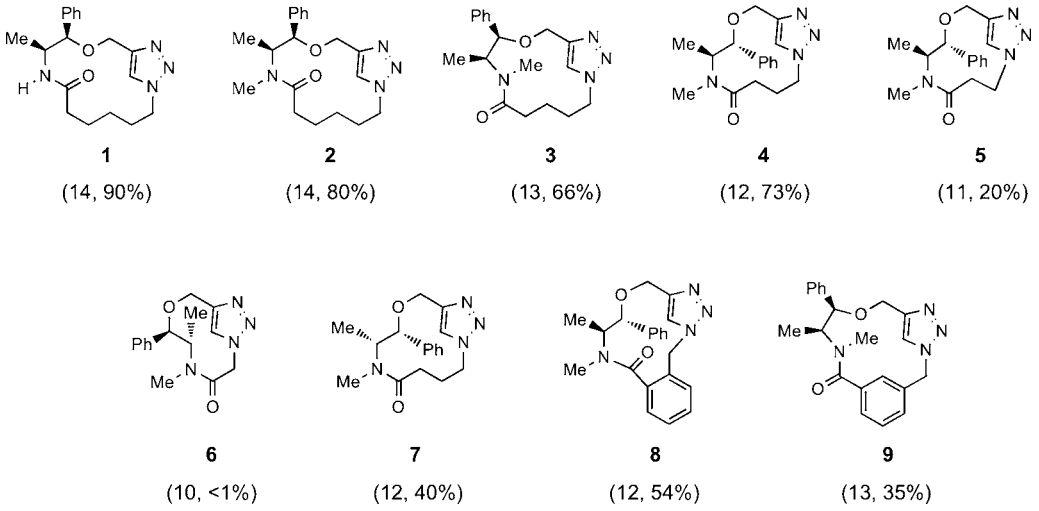

Figure 1. Macrocycles prepared by CuAAC macrocyclization in flow. Ring size and yield indicated in parentheses. No specific amide bond geometry is intended.

macrocycles therefore have potential value in tackling novel types of molecular targets.

We now report a systematic study of a series of strained, drug-like cyclophane macrocycles. We have explored the consequences of progressively increasing macrocyclic ring strain for their synthesis and structure and have established a basis for predicting which members of a larger virtual library of macrocycles would be synthetically accessible via this route.

RESULTS AND DISCUSSION

We recently reported a method for generating what we defined as drug-like macrocycles *via* an intramolecular copper catalyzed azide−alkyne cycloaddition (CuAAC) reaction conducted in flow, using a heated copper tube.[7] This protocol allows the macrocycles to be prepared in useful quantities under modest dilution and has been used successfully to generate macrocycles as large as 29-membered rings in good yield. The reaction generates a 1,4-disubstituted 1,2,3-triazole, a stable, drug-like functional group possessing geometric and H-bond acceptor properties which render it isosteric with a trans-amide bond.[10]

We have now applied this methodology to the synthesis of a homologous series of macrocycles containing 10- to 14-membered rings, in order to determine the structural properties of these systems and the lower limit of macrocycle ring size accessible *via* this approach (Figure 1). We presumed that this lower limit would be dependent upon the substitution pattern of the ring and would be governed by the point at which the incipient ring strain in the macrocycle would significantly reduce the rate of the macrocyclization reaction in comparison to the dimerization. The flow synthetic approach used was ideal for taking precise measurements of the macrocycle-to-dimer ratio, *via* UV spectroscopy, of reaction segments emerging from the flow reactor.

The majority of the macrocycles are based upon the homochiral (1*R*,2*S*)-ephedrine fragment. This common core provided a set of reference atoms through which we could compare the structures of the homologous macrocycles. It also constituted a useful bifunctional amino alcohol building block, which allowed incorporation of the requisite alkynyl and azido-functional groups *via* a short synthetic sequence. Additionally, we could readily access the diastereoisomeric and homologous homochiral fragments, (1*R*,2*R*)-pseudoephedrine and (1*R*,2*S*)-norephedrine respectively, with which we could examine the effect of changes in stereochemistry as well as transannular interactions. The synthesis of each macrocycle precursor followed an analogous route (Scheme 1a). The only departures involved the 10-membered system, where the azido-group was introduced in the final step (Scheme 1b), and the 11-membered system, where β-elimination issues necessitated use of a diazo-transfer reagent on a β-amino acyl system (Scheme 1c) (full experimental details are provided in the Supporting Information).

Scheme 1. Synthetic Routes to Azido-alkyne Precursors for CuAAC Macrocyclizations[a]

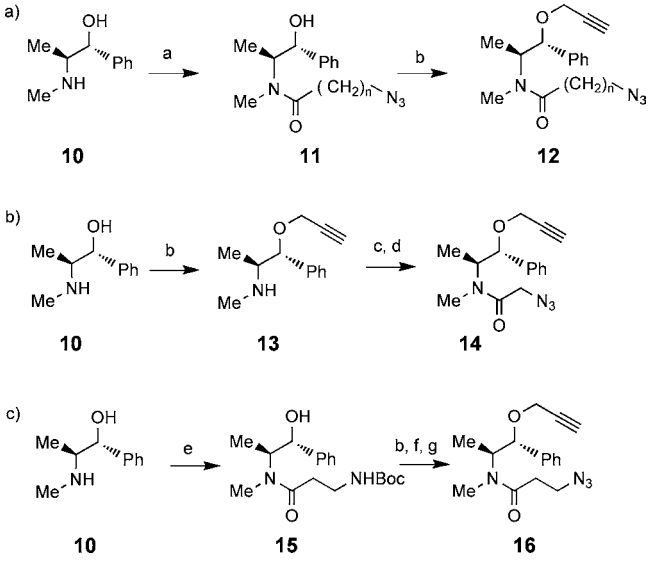

[a](a) N_3-$(CH_2)_n$-CO_2H, PyBOP, DIPEA, DMF. (b) NaH, propargyl bromide, THF. (c) Chloroacetic anhydride, TEA, CH_2Cl_2. (d) NaN_3, MeCN (aq). (e) N-Boc-β-alanine, PyBOP, DIPEA, DMF. (f) HCl, Dioxane. (g) Imidazole 1-sulphonyl azide hydrochloride, $CuSO_4{\cdot}5H_2O$, K_2CO_3, MeOH.

The structures of all macrocycles successfully isolated (all but **6**) were determined by X-ray crystallography, in order to allow accurate measurement of bond angles and lengths. Geometry

dx.doi.org/10.1021/ja208503y | J. Am. Chem.Soc. 2012, 134, 2127−2138

optimizations were conducted for all the macrocycles at the B3LYP/6-31+G(d) level of theory. It is known that B3LYP and related density functionals do not include dispersion energy, and this may introduce significant errors in comparing different structures that have varying nonbonded interactions. Dispersion corrections were therefore added through Grimme's D3 procedure, since these provide considerably better energetics for such systems. Gas-phase enthalpies for each compound were computed from calculated vibrational frequencies at 298 K. Using standard statistical formulas, gas-phase entropies were also computed. Entropic effects have a minimal impact on calculation of strain and are left for discussion in the Supporting Information

Side-by-side comparison of computed (left) and experimental structures (right) for all compounds are displayed in Figure 2. Several specific geometrical features from experiment and theory are compared in Table 1. Where we could make a comparison, the global minima were mostly in excellent agreement with the experimental X-ray data. The exceptions were as follows. In the 13-membered macrocycle **3**, the puckering of the ring and the distortion of the amide differed significantly between X-ray and computed structures. Thus, we find a 16.0° deviation from planarity of the amide in the X-ray structure compared with only a 2.7° distortion in the computed structure. In all other ephedrine derivatives possessing a trans-amide bond (**1**−**5** and **7**−**8**), the deviation of the amide was found not to exceed 5° between computed and X-ray structures. This larger deviation in **3** cannot be readily accounted for. Macrocycle **9** was the only case in which the lowest energy computed structure contained a cis-amide bond, whereas the X-ray structure exhibited a trans-amide bond. Finally, macrocycles **2** and **7** exhibited a difference in the rotation of the triazole between computed and X-ray structures. These cis-*versus* trans-amide and triazole-rotamer issues are discussed more fully below.

We also computed the strain energies of each of the macrocyclic compounds in two ways. First, we compared the energies of hydrogenation of each of the optimized cyclic structures and compared those heats of hydrogenation with those of an unstrained compound. The strain energies were also calculated by computing the energies of reaction of the azide−alkyne cycloadditions leading to macrocycles and by comparing those to the energies of reaction for an acyclic system. Strain

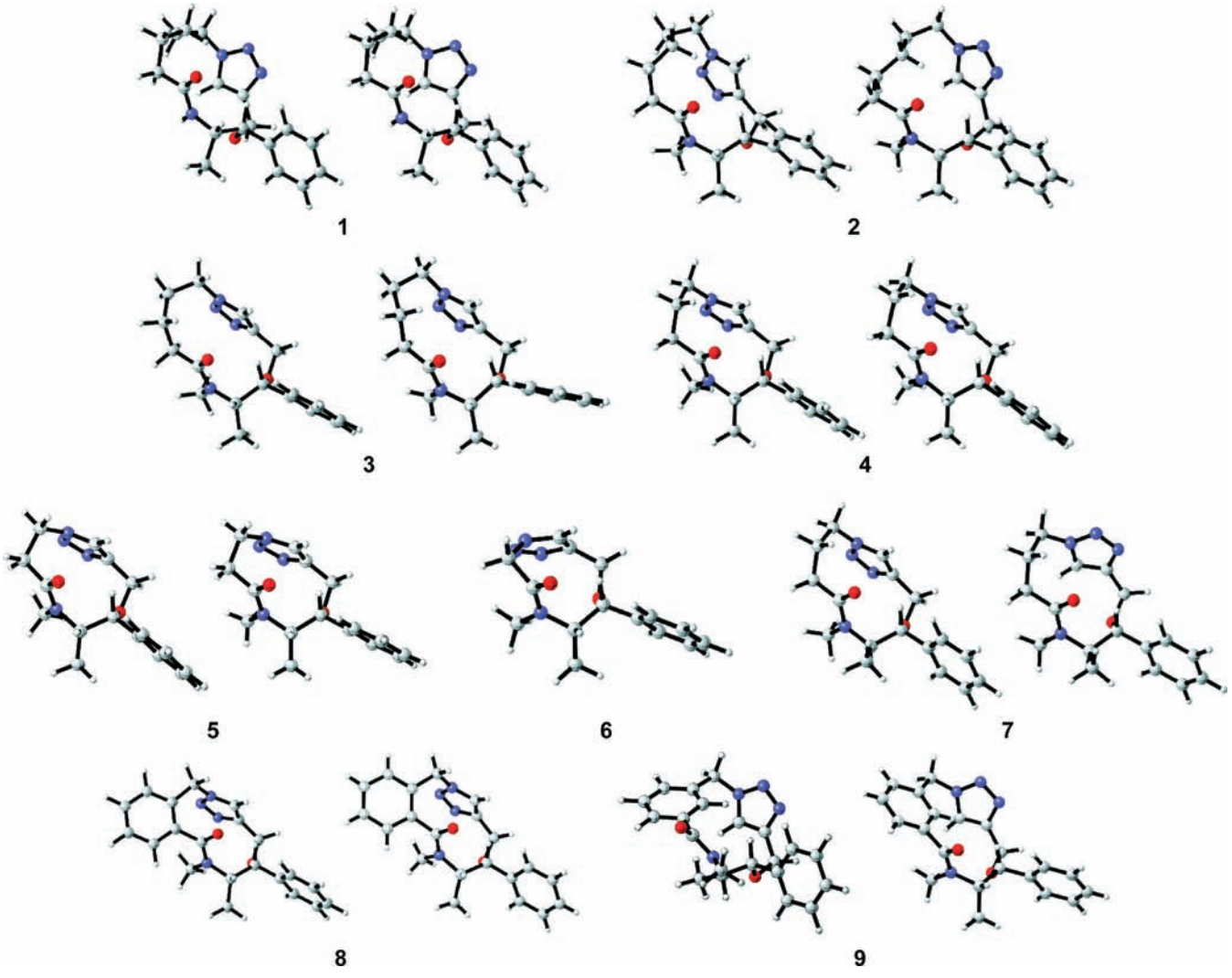

Figure 2. Computed (left) and X-ray (right) global minimum structures. The perspective for each pair is aligned by superimposition of the amide carbonyl, carbon, and nitrogen atoms. Only the calculated structure **6** is displayed.

dx.doi.org/10.1021/ja208503y | *J. Am. Chem.Soc.* 2012, 134, 2127−2138

Table 1. Summary of Macrocycle Yields, Strain Energies, and Selected X-ray Crystallographic Measurements (Computed Values in Parentheses)

Compd	Ring Size	Product to Dimer Ratio[a]	Isolated Yield (%)	Strain via Enthalpiesof Hydrogenation (kcal/mol)	Strain via Enthalpies of Reaction (kcal/mol)	Average Strain (kcal/mol)	Triazole Distortion[b] (180-α) (deg)	Triazole Distortion[c] (180-β) (deg)	Amide Distortion[d] (180-γ) (deg)
1	14	13.7:1	90	−0.8	−2.6	−1.7	2.0 (7.5)	0.4 (5.1)	5.9 (1.7)
2	14	6.7:1	80	−2.9	−1.9	−2.4	9.2 (5.9)	6.6 (3.8)	2.6 (3.5)
3	13	2.4:1	66	0.0	0.7	0.4	4.0 (3.1)	1.6 (5.9)	16.0 (2.7)
4	12	4.6:1	73	1.0	2.2	1.6	7.0 (9.6)	12.0 (11.9)	4.4 (3.6)
5	11	0.49:1	20	4.1	6.0	5.0	25.5 (26.1)	18.1 (19.5)	5.9 (4.3)
6	10	0.02:1	<1	21.9	24.3	23.1	(43.0)	(30.2)	(28.6)
7	12	1.6:1	51	−3.4	−2.3	−2.8	10.6 (12.5)	9.1 (12.0)	2.2 (1.0)
8	12	1.9:1	54	−2.9	5.2	1.2	13.4 (13.0)	14.3 (14.9)	10.5 (10.7)
9	13	1.2:1	35	4.4	11.1	7.7	21.5 (19.3)	8.8 (14.8)	30.6 (3.2)

[a]Ratio of macrocycle to dimer determined by UV spectroscopy. [b]Dihedral NNNC angle α (defined in Figure 4) measures out-of-plane bend of N_1-substituent on triazole. Numbers in parentheses are from calculations. [c]Dihedral NNCC angle β (defined in Figure 4) measures out-of-plane bend of C_4-substituent on triazole. Numbers in parentheses are from calculations. [d]Dihedral CCNC angle γ measures torsion about N−C(O) bond of amide. Numbers in parentheses are from calculations.

was then calculated using the equation $\Delta\Delta H(\text{Strain}) = \Delta H_{rxn}(\text{Unstrained Model}) - \Delta H_{rxn}(\text{Macrocycle})$ (Figure 3).

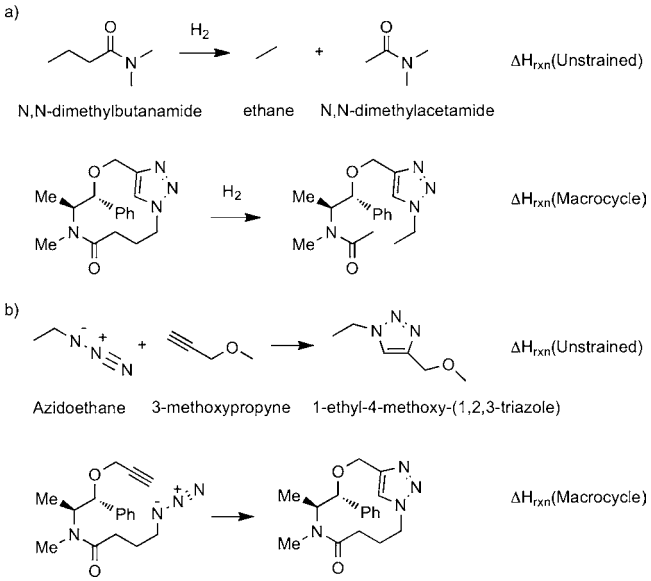

Figure 3. (a) Reference hydrogenation reactions used to calculate macrocycle strain energies. (b) Reference cycloaddition reactions used to calculate strain energies.

Inspection of the X-ray crystal structures revealed distortions in the macrocyclic ring, which became more pronounced as the strain energy increased. In particular, the bonds to the triazole ring are bent out of plane and the amide is distorted from planarity. The distortion observed for these functional groups, the strain energies computed *via* both methods, an average strain energy (from the two different calculation methods) for each molecule, macrocycle-to-dimer ratios, and isolated yields are summarized in Table 1. The angular distortions in the last three columns are discussed below.

Impact of Ring Size. The norephedrine-derived 14-membered macrocycle **1** represents a low strain system in which the triazole ring and amide bond are both almost planar. The dihedral angles used to determine distortion are defined in Figure 4. It is notable that it was generated in 90% isolated yield. The ephedrine-derived 14-membered macrocycle **2**,

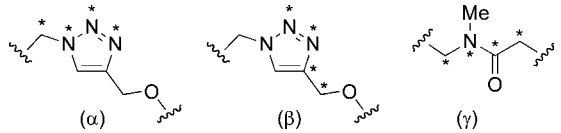

Figure 4. Dihedral angles used to calculate distortion of triazole and amide.

(compared with **1** in Figure 5) is the *N*-methylated analog of **1**. It was obtained in slightly lower, but still high, yield (80%).

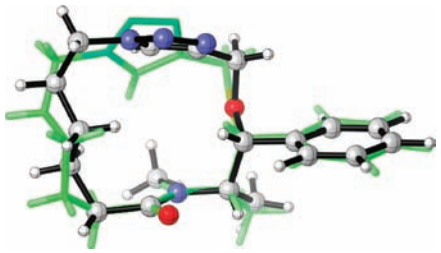

Figure 5. Superposition of macrocycles 1 (green) and 2 at the amide oxygen, carbon, and nitrogen atoms (X-ray).

The strain energy of this system is comparable. Interestingly, there is now a 15.8° distortion from planarity evident across the triazole system (sum of columns 8 and 9 in Table 1), and the macrocycle has adopted a slightly different pucker in order to avoid a steric clash between the triazole C-5 proton and the amide N-methyl group now present in this system, as illustrated in Figure 5. The distance between the amide nitrogen atom and the triazole C-5 carbon has increased from 3.6 Å in the norephedrine-derived macrocycle to 4.3 Å in the more congested ephedrine-derived macrocycle.

The next lower homologue **3** in the ephedrine series, containing a 13-membered ring, shows a modest increment in strain energy (average 2.8 kcal/mol) compared to the 14-membered homologue. As illustrated in Figure 6, the relative orientation of the triazole ring and amide bond have now reversed compared to the higher homologue, presumably, in order to avoid an even more pronounced steric clash between the triazole C-5 proton and the amide N-methyl group noted above. Despite the slight increase in strain energy compared to its higher homologue, the distortion of the triazole ring is less

dx.doi.org/10.1021/ja208503y | J. Am. Chem.Soc. 2012, 134, 2127−2138

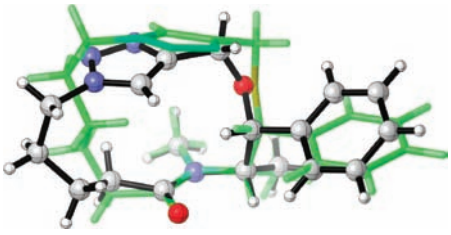

Figure 6. Overlap of 13-membered macrocycle **3** and 14-membered macrocycle **2** (green). Molecules are superimposed at the amide oxygen, carbon, and nitrogen atoms (X-ray).

pronounced in this 13-membered ring, perhaps because of the flip in orientation. Instead, there is much greater deformation of the amide bond, which is 16° out of planarity.

Since we had now observed two different conformations of the triazole ring in relation to the amide bond, we have adopted a convention of describing the triazole conformer which places the triazole N-2 and N-3 atoms on the same face of the macrocycle as the amide carbonyl oxygen as ***syn*** (as in the norephedrine 14-mer and ephedrine 14-mer X-ray structures) and the confomer which places these groups on opposite faces of the macrocycle as ***anti*** (as in the ephedrine 13-mer X-ray structure).

The 12-membered system **4** was also generated in good yield and exhibits a broadly similar conformation to the 13-membered macrocycle **3** (Figure 7). Strain has once again

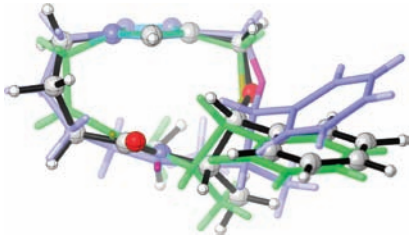

Figure 7. Overlap of 12-membered macrocycle **4**, 11-membered macrocycle **5** (green), and 13-membered macrocycle **3** (blue), illustrating progressive distortion across the triazole ring (viewed edge on). Molecules are superimposed at the amide oxygen, carbon, and nitrogen atoms (X-ray).

increased slightly, although it still modest. Upon examination of the crystal structures, it is surprising, however, that in this case the triazole ring exhibits most of the distortion resulting from the increase in strain (19° deviation from planarity), with the amide bond appearing much closer to planarity (4° deviation) than in the 13-membered ring.

The 11-membered macrocycle **5**, which by the earlier definition is strictly a medium-ring system, proved to be significantly more strained and much more challenging to synthesize. The macrocyclization reaction was further diluted in this case in order to improve the isolated yield, but even so, the macrocycle was now generated in only 20% yield. The average strain energy is >7 kcal/mol higher than the 14-membered homologue, and the X-ray structure of this system now shows significant deviation from planarity across the triazole system (43°) in order to accommodate this strain (Figure 8). The relative orientation of triazole and amide bonds matches that of the 12- and 13-membered rings (Figure 7). This molecule is the first 11-membered ring cyclophane reported containing a 1,4-disubstituted 1,2,3-triazole. There has been one earlier report of

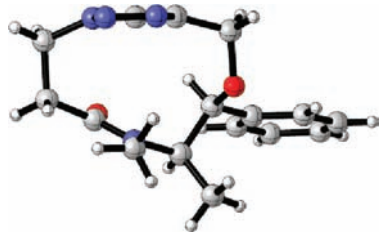

Figure 8. Edge-on view of 11-membered macrocycle **5**, illustrating the significant distortion across the triazole ring. Dihedral angles α = 155° and β =162° (X-ray).

an 11-membered ring containing a 1,5-disubstituted 1,2,3-triazole, which was the surprising product of a CuAAC reaction expected to produce a 12-membered 1,4-triazole system.[11] In that case, it was concluded that the nonbridged 11-membered ring was less strained than the intended bridged 12-membered ring, although the generation of a 1,5-disubstituted system under copper catalyzed conditions is clearly highly unusual. Our copper catalyzed reaction yielded the expected 1,4-triazole product, which we would expect to be more strained than the 11-membered ring generated in this literature report, by virtue of the additional challenge of accommodating the 1,4-disubstitution pattern across the triazole ring.

Our attempt to generate **6**, possessing a 10-membered ring, was unsuccessful. Although a small peak was visible in the LC/MS trace of the reaction segment, it represented a less than 1% yield, with the starting material having been converted to a dimer and other higher-order oligomers. The average calculated strain energy for this system is now >25 kcal/mol higher than the 14-membered homologue, and it appears that the azido-alkyne substrate proceeds almost exclusively along alternative intermolecular reaction pathways to yield less strained products.

Impact of Stereochemistry. Since changes in substrate stereochemistry are known to affect the outcome of macrocyclizations,[12] we also explored the impact of changing the configuration at the stereogenic center bearing a methyl group in the 12-membered ephedrine-derived macrocycle **4**. Thus, the corresponding pseudoephedrine-derived macrocycle **7** was generated, albeit in slightly lower yield than its diastereoisomer **4**. As illustrated in Figure 9, its X-ray structure did indeed reveal a

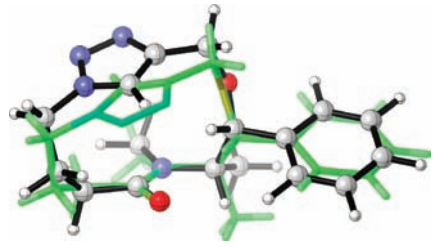

Figure 9. Overlap of 12-membered macrocycle **7** derived from pseudoephedrine (green) and 12-membered macrocycle **4** derived from ephedrine. Molecules are superimposed at the amide oxygen, carbon, and nitrogen atoms (X-ray).

significant conformational change in the 12-membered macrocycle. Relative to the amide bond, the triazole ring has flipped from the anticonformer into the syn-arrangement that had hitherto been observed in the larger, 14-membered rings. In this case it is difficult to rationalize why this change in stereochemistry at one ring position should lead to the

dx.doi.org/10.1021/ja208503y | J. Am. Chem.Soc. 2012, 134, 2127−2138

Table 2. Relative Enthalpies of Cis *versus* Trans Amide and Syn *versus* Anti Triazole Conformers (kcal/mol), Computed with B3LYP/6-31+G(d)[a]

Compd	Ring Size	*Cis-Syn* Relative Enthalpy (kcal/mol)	*Cis-Anti* Relative Enthalpy (kcal/mol)	*Trans-Syn* Relative Enthalpy (kcal/mol)	*Trans-Anti* Relative Enthalpy (kcal/mol)	ΔH(Cis)-ΔH(Trans) (kcal/mol)	ΔH(Syn)-ΔH(Anti) (kcal/mol)
1	14	13.7	12.2	0.0*	0.2	12.2	−0.2
2	14	12.2	11.0	1.5*	0.0	11.0	1.5
3	13	9.6	11.0	6.0	0.0*	9.6	6.0
4	12	12.6	11.2	2.5	0.0*	11.2	2.5
5	11	15.1	13.7	6.2	0.0*	13.7	6.2
6	10	11.7	9.9	4.5	0.0	9.9	4.5
7	12	9.0	5.4	1.1*	0.0	5.4	1.1
8	12	15.1	14.0	4.1	0.0*	14.0	4.1
9	13	0.0	11.4	0.7*	0.5	−0.5	−0.5

[a]Lowest energy conformer for each compound defined as 0 kcal/mol. X-ray conformation indicated by asterisk.

adoption of such a different conformation for the 12-membered ring. The strain energy of this system is low, and therefore we attribute the lower yield observed relative to its diastereoisomer as a kinetic effect, whereby the arrangement of methyl, phenyl, azido, and alkynyl substituents in the linear precursor is less favorable for achievement of the transition state for cyclization in the case of macrocycle **7** compared with macrocycle **4**.

In order to explore this change in triazole conformation in more detail, we calculated the relative energies of both triazole conformers for all nine macrocycles (Table 2). Additionally, in order to ensure a comprehensive picture of conformational preferences in these systems, we also determined the relative energies of the cis-amide rotamer for each triazole conformer. It is noteworthy that all the X-ray structures exhibited a trans-geometry for the amide bond, even though the amide is tertiary in all but **1**, and so the energy cost of adopting a cis-conformation would be minimized. As Table 2 illustrates, apart from molecules **1** and **9**, the majority of the macrocycles would be expected to exhibit a preference for the *trans-anti* conformer. However, in the case of macrocycles **2** and **7**, where the *trans-syn* conformer is observed in the X-ray structure, the energy difference is small and could readily be compensated for by crystal packing forces. Thus, the apparent difference in triazole conformation observed upon changing the stereochemistry of macrocycle **4** (derived from ephedrine) to yield macrocycle **7** (derived from pseudoephedrine) is probably an artifact of crystal packing.

Impact of Conformational Constraint. Since it was not possible to increase ring strain further by ring contraction or a change in stereochemistry, we examined an alternative approach, involving conformational constraint of the ring atoms. The benzo-fused system **8** was prepared by incorporation of an *o*-(azidomethyl)benzoyl substituent into the macrocyclization precursor in place of a simple azido-alkanoyl moiety. This yielded a 12-membered macrocycle in which two carbon atoms were also part of a benzene ring. Surprisingly, although generated in a slightly lower yield than the corresponding nonbenzo-fused system **4**, macrocycle **8** did not appear to be more strained (Table 1, entry 8 versus 4). Comparison of the X-ray structures, as illustrated in Figure 10, showed a very close correspondence, indicating that the transformation of the two adjacent sp^3 centers into sp^2 centers by incorporation of the ortho-fused benzene ring does not represent a significant perturbation for the macrocyclic ring.

In contrast, incorporation of a *m*-bridged benzene ring resulted in a profound change in macrocycle conformation and

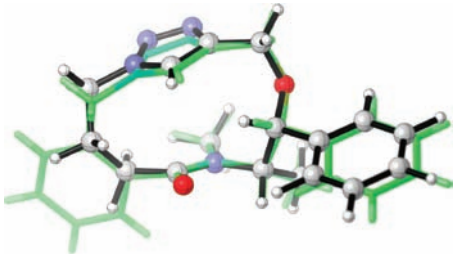

Figure 10. Overlap of 12-membered macrocycle **4** and 12-membered benzo-fused macrocycle **8** (green). Molecules are superimposed at the amide oxygen, carbon, and nitrogen atoms (X-ray).

behavior. Thus, the benzo-bridged system **9** was generated *via* incorporation of a *m*-(azidomethyl)benzoyl substituent in the macrocyclization precursor. This yielded 13-membered macrocycle **9** in low yield, although still slightly higher than that of the 11-membered system. Its average strain energy is >7 kcal/mol higher than the nonbridged 13-membered macrocycle **3**. As illustrated in Figure 11, like the 11-membered macrocycle **5**,

Figure 11. Overlap of 13-membered *m*-benzo-bridged macrocycle **9** and 13-membered macrocycle **3** (green). Molecules are superimposed at the amide oxygen, carbon, and nitrogen atoms (X-ray).

compound **9** shows significant distortion of both the triazole ring and amide bond (>30° deviation from planarity in both cases). In addition, the amide carbonyl is not conjugated with the aromatic ring, due to rotation around the (aryl)−C−(CO)C bond.

Relationship of Structure to Conformational Flexibility. Although access to X-ray crystallographic data has enabled us to understand the impact of ring size on strain energy and structural deformation within this series of macrocycles, NMR data, particularly for macrocycle **9**, suggested that the static X-ray structures provided only a partial description of these systems, which appeared to exhibit dynamic exchange behavior in solution.

dx.doi.org/10.1021/ja208503y | *J. Am. Chem.Soc.* 2012, 134, 2127−2138

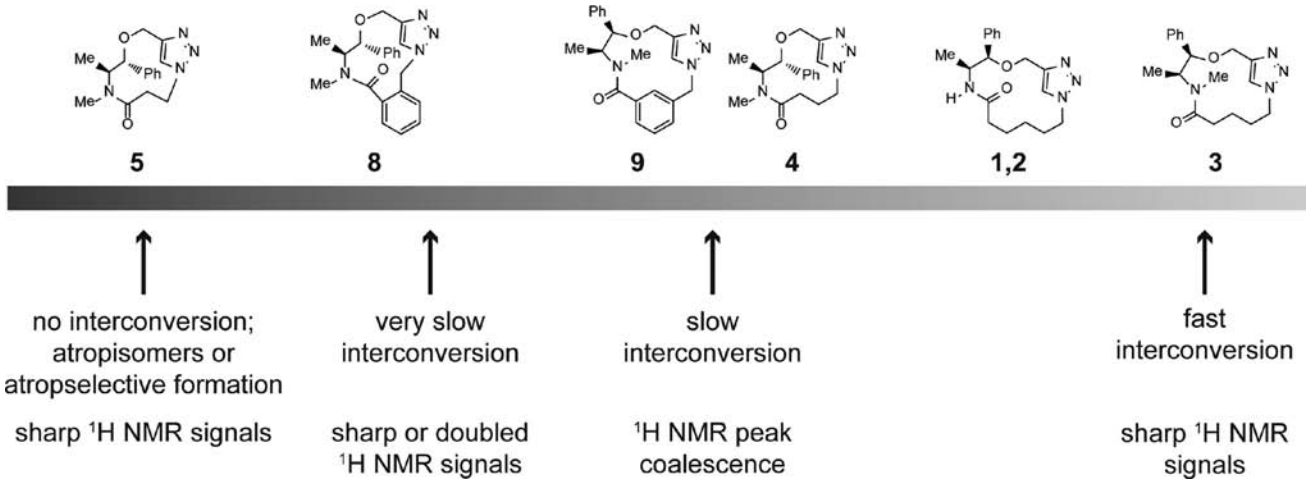

Figure 12. Continuum of conformational exchange rates indicating qualitative differences in behavior between macrocycles with differing degrees of conformational constraint.

Comparison of ^{1}H and ^{13}C NMR spectra for members of the series revealed differences in line shape, the presence of multiple species, and response to elevated temperature, which were indicative of differing degrees of conformational mobility (see Supporting Information for spectra and qualitative analysis). In particular, although only a single conformer of the triazole ring was observed in the unit cell for each of the X-ray structures (although the particular conformer was variable), it appeared that under some circumstances both possible conformers could be present in solution. Based upon these observations, we constructed a qualitative representation of where members of this macrocyclic series sit on a hypothetical continuum of conformational exchange rates, as illustrated in Figure 12.

Macrocycle **9** occupies approximately the center of this continuum based upon the following analysis. Although the X-ray crystal structure of macrocycle **9** contains a single molecular species in the unit cell, it was evident from the ^{1}H NMR spectrum of this molecule that there were three distinct species present in solution in an approximate ratio of 7:1:1. Figure 13a illustrates the upfield region of the 400 MHz ^{1}H NMR spectrum in d_6-DMSO at 30 °C, in which three signals arising from the methyl group are visible. A similar pattern of three related signals was also evident in other regions of the spectrum (see Supporting Information for full spectroscopic details). This suggested the presence of three conformers of similar but unequal energy, which undergo slow conformational exchange on the NMR time scale. In order to characterize this unusual system, we therefore conducted a series of additional NMR experiments.

First, we performed a variable temperature (VT) NMR experiment in which the solution was heated and spectra were measured at temperature increments from 30 to 80 °C, as illustrated in Figure 13b. The series of spectra illustrate that as the temperature is raised, the signals coalesce and that by 80 °C there is a single signal, corresponding to an averaging of the original signals, indicative of rapid conformational exchange now between the three species present. The coalescence point for the exchange appears to be between 70 and 80 °C. Although it is possible to derive kinetic information about such an exchange process from VT NMR studies on simple, binary systems,[13] the complexity of the current system (three interconverting species in unequal proportions) meant that this was not possible. We therefore ran an EXSY experiment[14] at 30 °C with a mixing time of 300 ms (together with a reference 'zero' mixing time of 3 ms), as illustrated in Figure 13c. This shows the clear presence of cross-peaks, indicating exchange between the three species, designated **A**, **B**, and **C**, which are slowly interconverting with the rate constants shown Figure 13d.

Based upon the sum of structural and energetic data gathered on this entire series of macrocycles, we envisaged the equilibrium illustrated in Figure 14 to account for these observations. Since, as discussed above, the triazole ring can exist in either *syn* or *anti* orientation with respect to the macrocyclic ring, and the tertiary amide bond can exist in either *cis* or *trans* conformations, there are four plausible conformations available to this molecule, **A**, **B**, **C** (observed by NMR) and **D** (not observed by NMR). These can interchange *via* a series of bond rotations, which result in flipping of the triazole ring and/or *cis*–*trans* isomerism of the amide bond. Since only three of the four possible conformers are observed in solution, we presume that the fourth, conformer **D**, is too high in energy to be populated to any extent. In order to unambiguously assign the identities of these four conformers, we have used a combination of computation and spectroscopic analysis.

As illustrated in Table 2 above, the calculated energies for these four possible conformations of macrocycle **9** reveal that while three of them are relatively close in energy, the *cis-anti* conformer is significantly higher in energy. This result is therefore consistent with the experimental observation of only three species in solution and identifies the nonobserved species **D** as the *cis-anti* conformer. Since the calculated energy differences between the other three conformers were small, we did not feel confident assigning their identities based only upon these data. We therefore looked for unique NMR signatures, which would be indicative of these structures. We hypothesized that the most abundant species was likely to be the *trans-syn* conformer observed in the X-ray structure. This assignment is supported by a trans-annular NOE between the proton attached to the triazole C-5 position and the protons of the amide *N*-methyl group. Based upon modeled conformations, this is the only species in which these protons are close enough to enable this interaction. We therefore assigned species **A** as the *trans-syn* conformer.

dx.doi.org/10.1021/ja208503y | *J. Am. Chem.Soc.* 2012, 134, 2127–2138

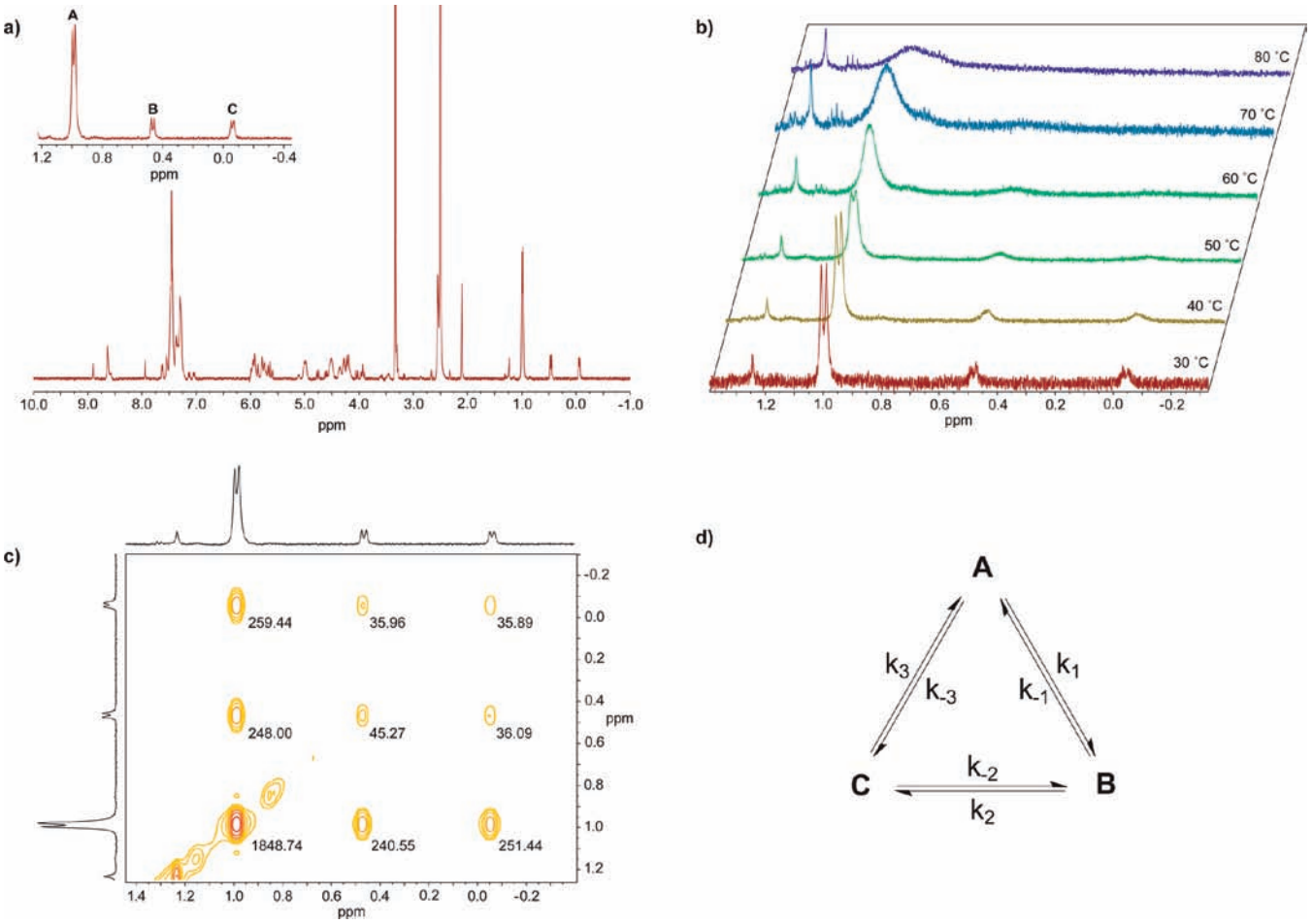

Figure 13. Dynamic exchange behavior of macrocycle **9**. (a) 400 MHz ^{1}H NMR spectrum at 30 °C in d_6-DMSO for macrocycle **9**. Expanded upfield region illustrating methyl group doublets from three interconverting species shown as insert. (b) Variable temperature 400 MHz ^{1}H NMR spectrum for macrocycle **9** in d_6-DMSO from 30 to 80 °C in 10 °C increments. (c) Expanded region of 400 MHz ^{1}H–^{1}H EXSY NMR spectrum at 30 °C in d_6-DMSO for macrocycle **9** (*Tm* 300 ms) illustrating cross-peaks and associated integrals arising from conformational exchange between methyl signals arising from three interconverting conformers. (d) Conformational equilibrium and rate constants for exchange between three conformers of macrocycle **9**, denoted **A**, **B**, and **C**.

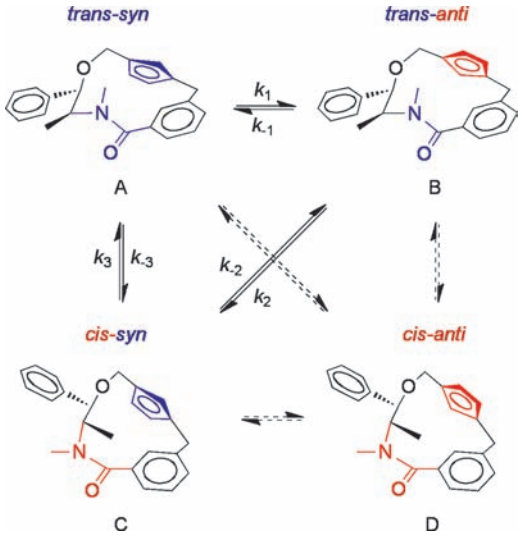

Figure 14. Perspective representations of the four possible conformers of macrocycle 9 (triazole nitrogens omitted for clarity), illustrating that whereas conformers **A**, **B**, and **C** are observed and in equilibrium with each other, conformer **D** is not observed.

We based the assignment of species **B** and **C** on the shifts of the signal for the methyl group doublet (Figure 13a). In the *cis-syn* conformer, this methyl group is close to the *m*-bridged aromatic ring. This results in shielding, which moves the signal corresponding to this methyl group upfield to −0.05 ppm. The corresponding methyl group in the other, *trans*-conformers is too far away from aromatic rings to experience such a shielding effect. We have therefore assigned species **C** as *cis-syn* and species **B** as *trans-anti*.

Table 3 shows the computed rate constants for the conformational exchange of macrocycle **9**. The data were

Table 3. Rate Constants for Conformational Exchange in Macrocycle 9 at 30 °C

	Conformational Exchange	rate constant (s^{-1})
k_1	A → B	0.95
k_{-1}	B → A	6.88
k_2	B → C	3.43
k_{-2}	C → B	3.39
k_3	C → A	19.80
k_{-3}	A → C	2.56

dx.doi.org/10.1021/ja208503y | *J. Am. Chem.Soc.* 2012, 134, 2127–2138

obtained using an $^1H-^1H$ EXSY pulse sequence on a 400 MHz spectrometer at 30 °C in d_6-DMSO (Figure 13c) and analyzed using the EXSYCalc program.[15] The exchange rates for transformation of conformations **B** and **C** to conformation **A** are more rapid than the conversion of conformation **A** to **B** and **C**, consistent with the higher abundance of **A** compared to **B** and **C** at 30 °C.[16] When the Onsager equation is applied to the rate data in Table 3 as a self-consistency check, the product is 1.08 (theoretical product = 1.0).[17]

In order determine how these rate constants changed with temperature, it was necessary to examine a lower temperature range,[16] which necessitated a switch of solvent to CD_3OD. Consequently, $^1H-^1H$ EXSY experiments were conducted at 10° increments from 273 to 303 K, generating a series of rate constants shown in Table 4. These were then used to calculate

Table 4. Rate Constants for Conformational Exchange in Macrocycle 9 between 273 and 303 K Determined by Variable Temperature EXSY Experiments

T (K)	k_1 (s^{-1})	k_2 (s^{-1})	k_3 (s^{-1})	k_4 (s^{-1})	k_5 (s^{-1})	k_6 (s^{-1})
303	1.24	3.18	0.61	2.4	11.92	1.53
293	0.39	1.07	0.53	1.51	7.93	1.10
283	0.12	0.32	0.22	0.48	2.75	0.43
273	0.03	0.07	0.07	0.12	0.74	0.13

activation parameters for the conformational exchanges in macrocycle **9** *via* the Eyring equation.[18] These are summarized in Table 5. The results reveal a significant negative $\Delta S^{\ddagger}$ value

Table 5. Activation Parameters for Conformational Exchange in Macrocycle 9, Calculated by Application of the Eyring Equation to Data in Table 4

Conformational Exchange	E_{act} (kcal mol^{-1})	$\Delta H^{\ddagger}$ (kcal mol^{-1})	$\Delta S^{\ddagger}$ (cal mol^{-1} K^{-1})	$\Delta G^{\ddagger}_{303}$ (kcal mol^{-1})
A → B	20.5	19.9	7.6	17.6
B → A	21.0	20.4	11.3	17.0
B → C	12.4	11.8	−20.0	17.9
C → B	16.8	16.2	−2.8	17.1
C → A	15.5	14.0	−3.8	16.1
A → C	13.9	13.2	−13.5	17.4

for the two transformations, B → C and A → C, both involving a *trans* to *cis* amide bond isomerization within the macrocycle ring. This suggests a requirement for a greater degree of organization in the transition states for these transformations, potentially involving a reduction in rotational degrees of freedom within the macrocyclic ring. The B → C exchange also involves a simultaneous flip of the triazole ring, perhaps in a concerted manner with isomerization of the amide. Despite these negative entropic changes, the overall free energy of activation for these two conformational changes is comparable with those associated with A → B and B → A exchanges, as a result of lower enthalpies of activation. This appears therefore to be an example of enthalpic/entropic compensation.[19]

In light of these spectroscopic findings, we have therefore placed macrocycle **9** just left of center upon the continuum depicted in Figure 12, since at room temperature it lies below its coalescence point in the 400 Mz NMR spectrum. In contrast, the 14-membered macrocycles **1**, **2** and the 13-membered macrocycle **3** occupy the right-hand end of the continuum, since the ring size and flexibility in these cases are sufficient to allow more rapid interconversion of triazole conformers at room temperature, which is manifest as a single set of signals in the NMR spectrum. Heating macrocycle **1** has no impact on NMR line shape up to 100 °C. The 11-membered macrocycle **5** occupies the left-hand end of the continuum. Even though it exhibits sharp signals in the ^1H NMR spectrum, it is much more rigid than **9** and cannot undergo conformational exchange. In fact, since there is only one species present in solution (i.e., the X-ray structure), it has been formed as a single atropisomer. The 12-membered macrocycle **4** sits on the continuum between the more flexible 14-membered macrocycle **1**, which is in fast exchange, and the less flexible, constrained 13-membered macrocycle **9**, which is in slow exchange. Thus, it shows broadening of lines in the NMR spectrum, but at room temperature it lies above its coalescence point, since heating results in line sharpening. We therefore placed the conformationally constrained 12-membered macrocycle **8** toward the left-hand end of the continuum, since it is more rigid than macrocycle **4** and yet shows a single sharp set of signals in the ^1H NMR spectrum. Once again, this macrocycle appears to have been formed as a single atropisomer.

The analysis suggests that, in this series, the rate of conformational exchange is governed by both macrocycle size and rigidity, with smaller, more rigid macrocycles trending toward slower exchange rates. It appears not to be a function of macrocycle strain energy *per se*, since macrocycle **8** appears to exhibit low conformational flexibility and very little ring strain. In those cases where a single conformer has been formed in the reaction, it appears that there is a significant energy difference between the transition states for the two possible atropisomeric macrocyclic products.

Impact of Strain on Macrocyclization Efficiency. The efficiency of the macrocyclization reactions at a given reaction concentration is reflected in both the product-to-dimer ratios (observed by UV spectroscopy) and the isolated yields of the macrocycle products after chromatography. A plot of product-to-dimer ratios and the isolated yields is illustrated in Figure 15, implying a logarithmic relationship. Since the UV method was based on an assumption that the extinction coefficients for macrocycle and dimer are equivalent, which cannot be guaranteed, we have used isolated yield as the preferred measure of macrocyclization efficiency. Isolated yields for cyclophane macrocycles were therefore plotted against the average strain energy (in kcal/mol) or the structural distortion (in degrees), as determined from the X-ray structure.

The variation in yield resulting from changes in ring strain across the homologous series is illustrated in Figure 16. There is a correlation with both average strain energy (Figure 16a) and structural distortion (Figure 16b). This correlation suggests that product structure/energy is a significant determinant of reaction outcome. Thus, as the strain energy of the product, and the transition-state, increase, the reaction is more likely to proceed along an alternative, intermolecular pathway, yielding dimer and higher-order oligomers. The equation describing the linear relationship between average strain energy and yield for this homologous series in Figure 16a is

$$\%\text{Yield} = -3.0(\text{Average Strain Energy}) + 62.9 \quad (R^2 = 0.69)$$

This suggests that the yield of a macrocyclization would reach 10% at a strain energy of 18 kcal/mol and 1% at a strain energy of 21 kcal/mol. Although we were not able to isolate the

dx.doi.org/10.1021/ja208503y | J. Am. Chem.Soc. 2012, 134, 2127−2138

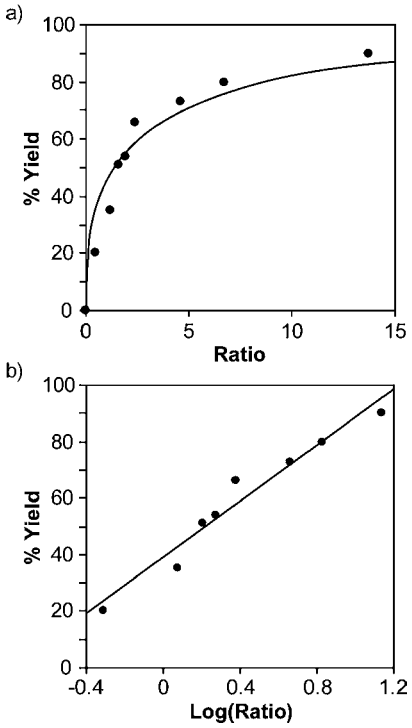

Figure 15. (a) Plot of isolated yield versus product-to-dimer ratio for compounds **1**−**5** and **7**−**9** (%Yield = 14.5*log(Ratio) + 46.3). (b) Plot of isolated yield versus logarithm of product-to-dimer ratio for compounds **1**−**5** and **7**−**9** (%Yield = 50.3*log(Ratio) + 38.0, R^2 = 0.95).

product of the macrocyclization to yield a 10-membered ring, we estimated its average strain energy by calculation to be >23 kcal/mol, which would be consistent with its production in only trace amounts. We therefore conclude that the generation of cyclophane macrocycles *via* a CuAAC macrocyclization is unlikely to be practical as the strain energy of the intended product approaches ∼21 kcal/mol.

Since both methods of assessing strain provide comparable correlations with yield, we conclude that the strain energy of these macrocyclic systems can be largely accounted for by perturbation of the triazole and amide geometries. This is demonstrated in Figure 16c, which shows a correlation (R^2 = 0.93) between the total distortion of the amide and triazole groups and the average computed strain energies. Finally, a plot of isolated yield versus enthalpy of reaction (Figure 16d) provides a similar picture to that obtained by plotting isolated yield versus strain energy. This is related to a Bronsted or Marcus relationship, where the rate of a reaction increases as the reaction becomes more exothermic.

CONCLUSION

Small macrocyclic rings represent an intriguing region of chemical space in which the intrinsic conformational constraint possessed by macrocycles is superimposed upon the geometric distortion exhibited by strained molecules. Although this domain has been explored to some extent in the context of natural product synthesis,[20] our results constitute an effort to systematically characterize how progressive changes in ring size and shape within a related series of macrocycles affect the likelihood of closing the macrocyclic ring and the structure of the resultant products. Our studies are based upon a homologous series of drug-like cyclophane macrocycles, designed to enable systematic exploration of incremental structural variations, which would not be straightforward in a natural product-based system, using a combination of X-ray crystallographic, spectroscopic, and computational approaches.

Decreasing the size of the ring, or introducing certain conformational constraints, resulted in diminished experimental yields and increased computed strain energies. The correlation between strain and experimental yield, shown in Figure 16a, while only qualitative, illustrates the eventual failure to generate the macrocyclic product when strain energy becomes too large. We observed this directly, since, for each of the macrocycles successfully synthesized, we predict strain energies less than 10 kcal/mol. In the case of the 10-membered ring macrocycle **6**, for which we calculate an average strain energy of >23 kcal/mol, macrocyclization is not observed. The smallest ring size successfully prepared, macrocycle **5**, is the first reported example of an 11-membered cyclophane containing a 1,4-triazole bridge and was generated as a single atropisomer with regard to the conformation of the triazole ring. Although we observed a qualitative correlation between macrocycle strain energy and isolated yield, there are clearly additional factors, such as kinetics, that impact the cyclization, since a stereochemical change did not increase macrocycle strain but nevertheless decreased yield. Our results suggest that, for CuAAC-macrocyclizations under these conditions, as strain energy approaches ∼21 kcal/mol, the reaction is likely to yield only oligomeric products.

The 13-membered macrocycle **9** beautifully illustrates the unusual properties of a strained macrocycle of small ring size. Our calculations show that it is the most strained macrocycle we were able to generate. Consistent with the correlation between calculated strain energy and X-ray derived structural distortion data, illustrated in Figure 16c, this molecule also shows the most significant perturbations in triazole and amide geometries. A consequence of this strain/distortion has been a closing of the energy gap between *cis*/*trans* and *syn*/*anti* conformers. As a result, it exists as a mixture of slowly interconverting conformers in solution at room temperature, which we have been able to characterize spectroscopically. This molecule thus approximately occupies the midpoint on a continuum of conformational exchange rates, as illustrated in Figure 12. Relaxing the degree of conformational constraint, or increasing macrocycle ring size, results in a rightward shift along the continuum to rapid conformational exchange rates where only single species are observed by NMR as a result of signal averaging. Tightening the degree of conformational constraint further, or decreasing macrocycle ring size, results in a leftward shift along the continuum to slow conformational exchange rates. Again, only single species are observed by NMR, but in this case because only a single atropisomer has been generated in the cycloaddition reaction.

The unusual architecture offered by the strained macrocycles generated *via* this procedure opens up new opportunities for the construction of geometrically novel molecules of potential pharmaceutical interest. Libraries based upon such systems would enhance molecular diversity by introducing distinct geometries, and therefore disposition of macrocycle substituents, rather than by the conventional means of connecting together atoms in a novel but strain-free configuration. Future studies will explore the utility of libraries of strained macrocycles in the discovery of leads against therapeutically important protein−protein interaction targets.

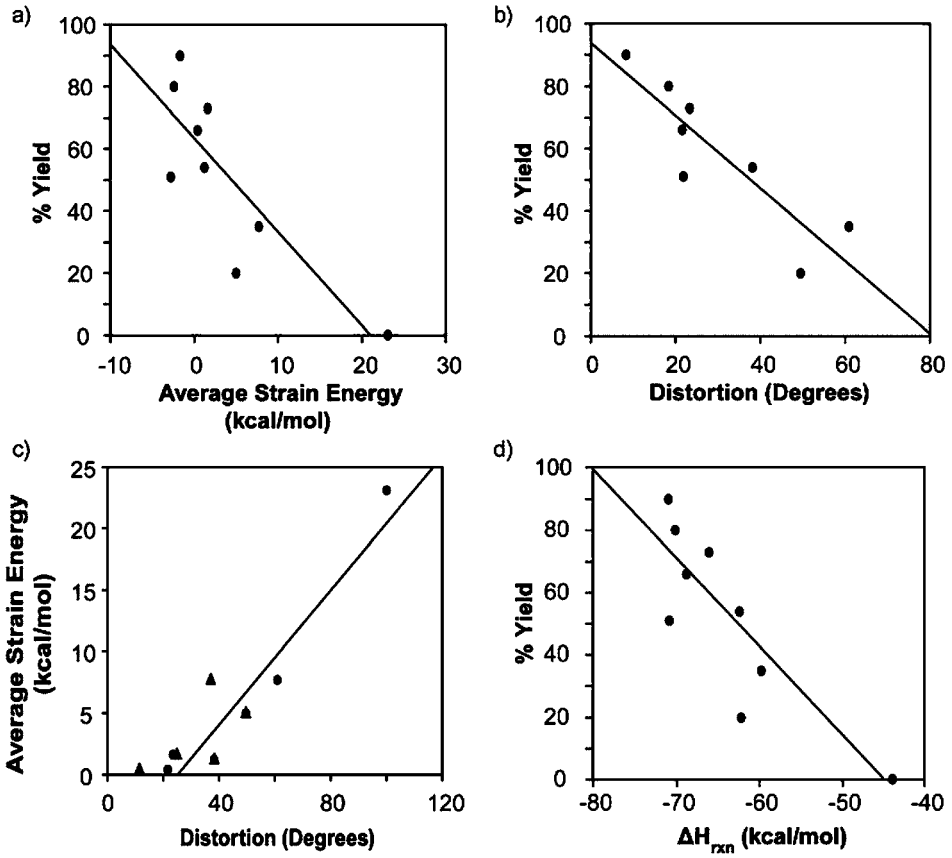

Figure 16. (a) Plot of isolated yield versus computed average strain energy for examples **1**–**9** (%Yield = −3.0*Strain Energy + 62.9, R^2 = 0.69). (b) Plot of isolated yield versus total distortion in X-ray structures for examples **1**–**5**, **7**–**9** (%Yield = −1.2*Distortion + 93.9, R^2 = 0.77). (c) Plot of computed average strain energies versus sum of amide and triazole distortion. Distortion calculated from experimental structures **1**–**5**, **7**–**9** represented by black circles and distortion from calculated structures **1**–**9** by triangles. (Strain Energy = 0.3*Experimental Distortion −6.8, R^2 = 0.93). (d) Plot of isolated yield for examples **1**–**9** versus enthalpy of reaction in kcal/mol (%Yield = −2.9*ΔH_{rxn} − 134.24, R^2 = 0.72).

EXPERIMENTAL SECTION

General Considerations. All reagents and solvents were used as received. THF was distilled from sodium. NMR spectra were recorded on a Bruker DRX-600, Bruker DRX-500, or Bruker AMX-400 instrument using a residual solvent peak as a reference. Data are reported as s = singlet, d = doublet, t = triplet, q = quartet, m = multiplet, br = broad. LC/MS analyses were carried out using an Agilent Technologies HPLC (Agilent Technologies 1100 Series diode array detector, Agilent Technologies 1100 Series column heater, Agilent 1100 Series pump, and Agilent 1100 Series degasser) interfaced with an Agilent Technologies 6110 Quadrupole LC/MS. Column chromatography was performed using a Biotage Horizon automated flash chromatography system equipped with a Biotage Horizon detector, fraction collector, and pump where noteed.

LC/MS Analysis. HPLC analyses was performed using a water (formic acid 0.1% w/v/ammonium formate 0.05% w/v) and MeCN (water 5% v/v, formic acid 0.1% v/v, ammonium formate 0.05% w/v) based gradient from 0 to 100% MeCN over 4 min. A Waters XBridge C18 2.5 μm (3.0 mm × 30 mm) column was used at 80 °C with a flow rate of 2.4 mL min^{-1}. Injections were made from diluted reaction mixtures, and ionization was monitored in positive or negative mode.

General Procedure for Preparative Scale Flow Macrocyclization. Azido-alkyne (0.10 M in EtOH, 100 μL, 0.010 mmol, 1.0 equiv), TTTA (0.01 M in EtOH, 100 μL, 0.001 mmol, 0.10 equiv), DIPEA (0.1 M in EtOH, 200 μL, 0.020 mmol, 2.0 equiv), and EtOH (200 μL) were aspirated from their respective source vials, mixed through a PFA mixing tube (0.2 mm inner diameter) and loaded into an injection loop. The reaction segment was injected into the flow reactor set at 150 °C and passed through the reactor at 300 μL min^{-1} (5 min residence time). A total of 40 reaction segments prepared in this manner were collected in a round-bottom flask. Upon completion, the reaction mixture was concentrated and dried *in vacuo*. The crude reaction mixture was purified using a Biotage Horizon automated flash column chromatography system (silica gel, EtOAc, R_f = 0.23) to yield **1** as an off-white solid (117.5 mg, 90% yield): ^{1}H NMR (600 MHz, $CDCl_3$): δ 7.72 (s, 1 H), 7.34–7.43 (m, 4 H), 7.27–7.31 (m, 1 H), 5.71 (d, J = 8.3 Hz, 1 H), 4.87 (d, J = 13.6 Hz, 1 H), 4.45–4.52 (m, 1 H), 4.38–4.44 (m, 2 H), 4.35 (d, J = 13.6 Hz, 1 H), 2.15–2.23 (m, 1 H), 1.77–2.00 (m, 4 H), 1.39–1.51 (m, 1 H), 1.21–1.30 (m, 2 H), 0.89 (d, J = 7.0 Hz, 3 H), 0.73–0.83 (m, 1 H); ^{13}C NMR (150 MHz, $CDCl_3$): δ 171.2, 145.5, 138.7, 128.4, 127.5, 126.6, 122.6, 80.1, 61.3, 50.1, 49.9, 34.5, 28.4, 23.6, 23.4, 12.3; HRMS (ESI-TOF): $C_{18}H_{24}N_4O_2$: $[M + H]^+$: calculated 329.1972, found 329.1975.

Computational Methods. Geometry optimizations were performed with the *Gaussian09*[21] electronic structure program at the B3LYP/6-31+G(d) level of theory. All single-point energies are corrected for dispersion interactions using the DFT-D3 method of Grimme and co-workers.[22] Frequency calculations verified that each structure was a minimum and provided thermal corrections to the electronic energies. All absolute energies are reported in hartrees, and relative electronic energies aregiven in kcal/mol. Energies of reaction are also reported in kcal/mol.

ASSOCIATED CONTENT

Supporting Information

Synthetic procedures and spectra for all molecules used in this study; X-ray crystallographic data for all macrocycles; ^{1}H-EXSY spectra and structural assignment for conformer of macrocycle **9**; qualitative NMR data analysis of macrocycles, used to derive

dx.doi.org/10.1021/ja208503y | J. Am. Chem.Soc. 2012, 134, 2127–2138

Figure 12; full list of authors for ref 21; spreadsheet of variable temperature ^{1}H-EXSY data used to generate Tables 4 and 5; coordinates for all computed and X-ray crystallographically determined macrocycle structures. This material is available free of charge via the Internet at http://pubs.acs.org.

AUTHOR INFORMATION

Corresponding Author

kjames@scripps.edu; houk@chem.ucla.edu

ACKNOWLEDGMENTS

We are grateful to the National Institutes of General Medical Sciences, the National Institutes of Health and Pfizer Worldwide R&D for their support and Academic Technology Services (ATS) at UCLA for access to the Hoffman2 cluster. We are also grateful to Jason Ewanicki (Pfizer) and Wei Wang (Pfizer) for assistance with VT and EXSY NMR experiments and Professor Tammy Dwyer (University of San Diego) and Dr Jordi Burés (The Scripps Research Institute) for advice on EXSY calculations. We thank Curtis Moore and Arnold Rheingold (UCSD Small-Molecule Lab) for X-ray crystallographic data.

REFERENCES

(1) (a) Driggers, E. M.; Hale, S. P.; Jinbo Lee, J.; Terrett, N. K. *Nat. Rev. Drug Discovery* **2007**, *7*, 608−624. (b) Marsault, E.; Peterson, M. L. *J. Med. Chem.* **2011**, *54*, 1961−2004.

(2) Wells, J. A.; McClendon, L. *Nature* **2007**, *450*, 1001−1009.

(3) For recent examples, see: (a) Dinsmore, C. J.; Bogusky, M. J.; Culberson, J. C.; Bergman, J. M.; Homnick, C. F.; Zartman, C. B.; Mosser, S. D.; Schaber, M. C.; Robinson, R. G.; Koblan, K. S.; Huber, H. E.; Graham, S. L.; Hartman, G. D.; Huff, J. R.; Wil, T. M. *J. Am. Chem. Soc.* **2001**, *123*, 2107−2108. (b) Shi, Z.-D.; Lee, K.; Liu, H.; Zhang, M.; Roberts, L. R.; Worthy, K. M.; Fivash, M. J.; Fisher, R. J.; Yang, D.; Burke, T. R. *Biochem. Biophys. Res. Commun.* **2003**, *310*, 378−383. (c) Udugamasooriya, G.; Saro, D.; Spaller, M. R. *Org. Lett.* **2005**, *7*, 1203−1206. (d) Tao, Z.-F.; Le Wang, L.; Stewart, K. D.; Chen, Z.; Gu, W.; Bui, M.-H.; Merta, P.; Zhang, H.; Kovar, P.; Johnson, E.; Park, C.; Judge, R.; Rosenberg, S.; Sowin, T.; Lin., N.-H. *J. Med. Chem.* **2007**, *50*, 1514−1527.

(4) Veber, D. F.; Johnson, S. R.; Cheng, H.-Y.; Smith, B. R.; Ward, K. W.; Kopple, K. D. *J. Med. Chem.* **2002**, *45*, 2615−2623.

(5) Rezai, T.; Yu, B.; Millhauser, G. L.; Jacobsen, M. P.; Lokey, R. S. *J. Am. Chem. Soc.* **2006**, *128*, 2510−2511.

(6) Wessjohann, L. A.; Ruijter, E. *Top. Curr. Chem.* **2005**, *243*, 137−184.

(7) Bogdan, A. R.; James, K. *Chem.—Eur. J.* **2010**, *16*, 14506−14512.

(8) Brandt, W.; V. Haupt, J.; Wessjohann, L. A. *Curr. Top. Med. Chem.* **2010**, *10*, 1361−1379.

(9) Meutermans, W. D. F.; Gregory T. Bourne, G. T.; Golding, S. T.; Horton, D. A.; Campitelli, M. R.; Craik, D.; Scanlon, M.; Smythe, M. L. *Org. Lett.* **2003**, *5*, 2711−2714.

(10) (a) Horne, W. S.; Olsen, C. A.; Beierle, J. M.; Montero, A.; Ghadiri, M. R. *Angew. Chem., Int. Ed.* **2009**, *48*, 4718−4724. (b) Beierle, J. M; Horne, W. S.; van Maarseveen, J. H.; Waser, B.; Reubi, J. C.; Ghadiri, M. R. *Angew. Chem., Int. Ed.* **2009**, *48*, 4725−4729.

(11) Ray, A.; Manoj, K.; Bhadbhade, M. M.; Mukhopadhyaya, R.; Bhattacharjya, A. *Tetrahedron Lett.* **2006**, *47*, 2775−2778.

(12) Lee, D.; Sello, J. K.; Schreiber, S. L. *J. Am. Chem. Soc.* **1999**, *121*, 10648−10649.

(13) Allerhand, A.; Gutowsky, H. S.; Jonas, J; Meinzer, R. A. *J. Am. Chem. Soc.* **1966**, *88*, 3185−3194.

(14) Perrin, C. L.; Dwyer, T. J. *Chem. Rev.* **1990**, *90*, 935−967.

(15) EXSYCalc application can be downloaded fro free from http://mestrelab.com/software/exsycalc/.

(16) Because of the large difference in abundance of the *trans-syn* conformer relative to the *cis-syn* conformer, and therefore the relatively high rate constant for the conformational change from *cis-syn* to *trans-syn*, our data are on the limit of what can be processed using the EXSYCalc algorithm. Thus, conducting the EXSY experiment at 40 °C generated data that could not be processed, presumably because the rate of conformational change is now outside the limits of the algorithm.

(17) (a) Blackmond, D. G. *Angew. Chem., Int. Ed.* **2009**, *48*, 2648−2654. (b) Onsager, L. *Phys. Rev.* **1931**, *37*, 405.

(18) Anslyn, E. V.; Dougherty, D. A. *Modern Physical Organic Chemistry*; University Science Books: Sausalito, CA, 2006.

(19) For discussion of this concept, see: (a) Exner, O. *Chem. Commun.* **2000**, 11665−1656. (b) Sharp, K. *Protein Sci.* **2001**, *10*, 661−667.

(20) For selected examples, see: (a) Braddock, D. C.; Millan, D. S.; Yolanda Pérez-Fuertes, Y.; Pouwer, R. H.; Sheppard, R. N.; Solanki, S.; White, A. J. P. *J. Org. Chem.* **2009**, *74*, 1835−1841. (b) Speicher, A.; Backes, T.; Hesidens, K.; Kolz, J. *Beilstein J. Org. Chem.* **2009**, *5*, 71. (c) Brown, M. K.; Hoveyda, A. H. *J. Am. Chem. Soc.* **2008**, *130*, 12904−12906. (d) Cluzeau, J.; Oishi, S.; Ohno, H.; Wang, Z.; Evans, B.; Peiperb, S. C.; Fujii, N. *Org. Biomol. Chem.* **2007**, *5*, 1915−1923. (e) Matsumura, T.; Akiba, M.; Arai, S.; Nakagawa, M.; Nishida, A. *Tetrahedron Lett.* **2007**, *48*, 1265−1268. (f) Tanabe, K.; Fujie, A.; Ohmori, N.; Hiraga, Y.; Kojima, S.; Ohkata, K. *Bull. Chem. Soc. Jpn.* **2007**, *80*, 1597−1604. (g) Collins, S. K. *J. Organomet. Chem.* **2006**, *691*, 5122−5128. (h) Wipf, P.; Furegati, M. *Org. Lett.* **2006**, *8*, 1901−1904. (i) Venkatraman, S.; Njoroge, F. G.; Girijavallabhan, V. *Tetrahedron* **2002**, *58*, 5433−5458.

(21) Frisch, M. J., et al. *Gaussian 09*, revision A.1; Gaussian, Inc.: Wallingford, CT, 2009.

(22) Grimme, S.; Antony, J.; Ehrlich, S.; Krieg, H. *J. Chem. Phys.* **2010**, *132*, 154104.